

# Overview of LIGO instrumentation

Frederick J. Raab\* (reporting for LIGO Scientific Collaboration)  
LIGO Hanford Observatory, P.O. Box 159, Richland, WA, USA 99352

## ABSTRACT

The Laser Interferometer Gravitational-Wave Observatory (LIGO) consists of detector facilities in Hanford, WA and Livingston, LA, USA, separated by 3000 km. Laser interferometry is used to monitor displacements of freely suspended mirrors, separated by 2 - 4 km, along perpendicular arms at each facility. The initial LIGO detector design sensitivity corresponds to measuring gravitational-wave induced differential displacements of order 1 millifermi over the 4-km arms. Progress in the commissioning and operation of these detectors will be reviewed.

Keywords: LIGO, gravitational waves

## 1. INTRODUCTION

The LIGO observatories in Hanford, Washington and Livingston, LA comprise the US effort to detect gravitational waves in the broad frequency band from a few hertz to several kilohertz [1]. LIGO is funded by the US National Science Foundation (NSF). The LIGO Laboratory has constructed (under cooperative agreement PHY-9210038) and now operates (under cooperative agreement PHY-0107417) the observatories and supporting facilities on the Caltech and MIT campuses. The LIGO Scientific Collaboration (LSC) conducts the scientific program for LIGO in coordination with the LIGO Laboratory. Currently, the LSC consists of more than 500 scientists and engineers worldwide. This review describes the work of my many colleagues within the laboratory and the collaboration.

The observatory facilities for LIGO have been completed and these are shown in figure 1. The Hanford Observatory is located on the US Department of Energy Hanford Site, in arid, shrub-steppe habitat approximately 25–30 km from the

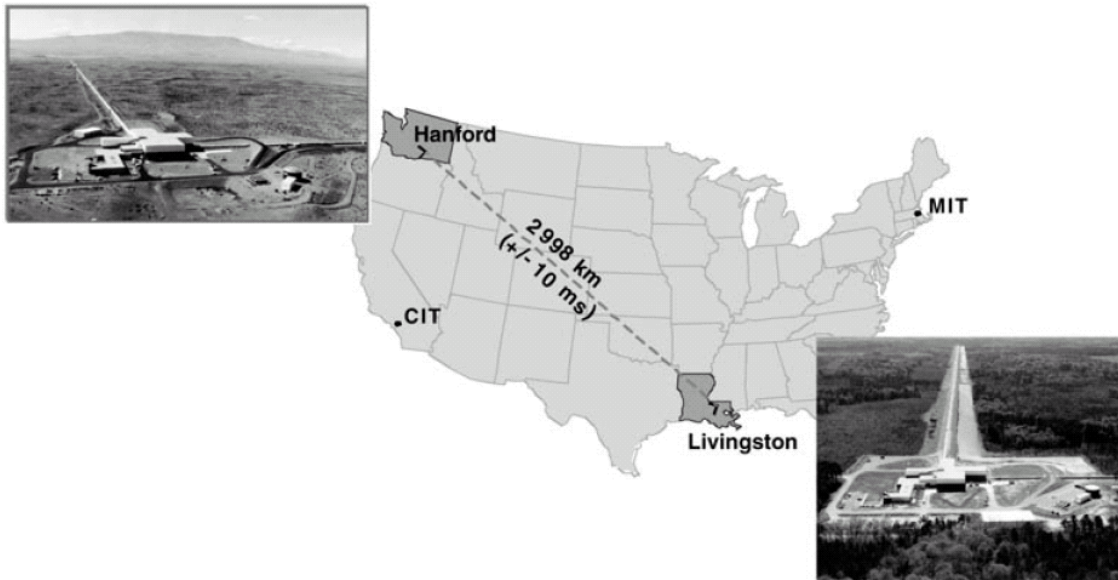


Figure 1: Locations and aerial views of observatories.

---

\* E-mail: [raab\\_f@ligo-wa.caltech.edu](mailto:raab_f@ligo-wa.caltech.edu); phone: 509-372-8125; FAX:509-372-8137.

cities of Richland, Kennewick and Pasco. The Livingston Observatory is located in forested land a similar distance from Baton Rouge. Each observatory has two perpendicular arms, 4 km long, spanned by 1.2 m diameter stainless steel vacuum tubing. Vacuum chambers, containing the vibration-isolation stacks and suspended mirrors for the 4 km interferometers, are within buildings at the corner and ends of the arms. The 4-km interferometer at Hanford is known as H1 and its twin at Livingston is known as L1. At Hanford, an additional 2 km interferometer, known as H2, shares the same vacuum tubing, with its end mirrors in buildings at the midpoints of the two arms. The observatories were oriented relative to each other to optimize detection of a common wave polarization. The facilities were designed to accommodate the most sensitive future detectors imaginable, allowing for broad-band detectors operating well below  $10^{-24}$  in strain at frequencies from 10 Hz to 10 kHz. The initial LIGO interferometers have been installed and three science runs, with significantly improving sensitivity, have alternated with periods of commissioning to improve detector performance. An advanced interferometer design will be described in tomorrow's session.

## 2. GENERAL PRINCIPLES

A gravitational wave produces a differential strain of space in planes transverse to the incident wave direction. This strain stretches (and shrinks) space along one axis in this plane while respectively shrinking (and stretching) space along the perpendicular axis in this plane. This will deform a circle of inertial frames in the plane of incidence into an ellipse. The difference between the semi-major axis and the semi-minor axes of the resulting ellipse at any instant of time, divided by the radius of the original circle, gives an operational definition of the instantaneous strain. In laser interferometer gravitational-wave detectors, suspended mirrors are used to approximate the inertial frames at the center of a circle and at two points on the circumference, separated by 90 degrees. A beam splitter is used as the central mirror to form a Michelson interferometer. Laser light illuminating the Michelson interferometer produces an interference pattern that gives a linear measure of the strain. The basic concept is sketched in figure 2.

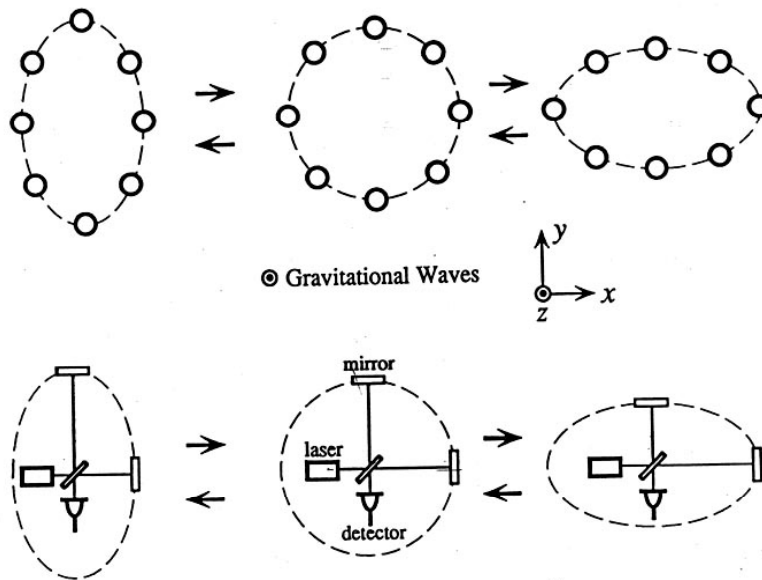


**Figure 2: Schematic of spatial distortion caused by an incident gravitational wave and its approximation by a suspended-mirror Michelson interferometer.**

The strains at Earth from astrophysical sources are expected to be less than  $10^{-21}$  RMS, a number comparable to the ratio of the thickness of a human hair to the distance between the Sun and Alpha Centauri. An interferometer with kilometer-scale arms thus requires a sensitivity to differential mirror displacements of  $\sim 10^{-18}$  m (or 1 millifermi) RMS. This corresponds to  $\sim 10^{-10}$  radians of optical phase. Residual seismic motion transmitted to the mirrors and the Brownian motion of the mirror and suspension structures in equilibrium at room temperature provide the natural background for these devices. The fundamental noise in sensing the interference is due to shot noise arising from the quantum nature of light. The relative complexity of these devices present many additional opportunities for noise to enter the system.

### 3. FACILITIES AND VACUUM SYSTEM

The LIGO facilities consist of buildings that house experimental equipment connected by vacuum tubes that conduct the laser beams between buildings. A corner-station building and two end-station buildings form the two arms of the interferometer. At Hanford there is an additional mid-station building centered on each arm to house the end mirrors of the 2-km interferometer. The arms have an opening angle of 90.00 degrees. The arms are configured to be straight and oriented as nearly transverse to Earth's gravitational acceleration as is reasonable, given Earth's curvature. The arms of the Hanford and Livingston facilities were aligned (modulo 90 degrees) to optimize sensitivity to the same polarization of gravitational wave within certain constraints imposed by the two sites. This allows optimal use of coincidence operation of the two interferometer sites to improve detection confidence.

Design choices in the facilities can limit the ultimate sensitivity of future detectors. Fluctuating gravity gradients on Earth produce a background that limits the frequency band of terrestrial gravitational-wave detectors to frequencies above  $\sim 10$  Hz. At frequencies above  $\sim 50$  Hz, fluctuations in the number of residual gas molecules transiting the light beams in the arms produce a fluctuating phase noise in the interferometers. In the middle range of frequencies, scattering between the mirrors and the beam tube walls can introduce noise caused by vibration of the beam tube walls.

The LIGO vacuum system consists of vacuum chambers that hold vibration-isolated optical platforms and the beam tubes along the arms. The evacuated chambers provide a quiet environment for the optics, eliminating acoustic coupling and reducing the Brownian motion of the mirrors from residual gas collisions to an acceptable value. The evacuated beam tube must mitigate against optical path length fluctuations due to residual gas and scattering from the beam-tube walls, which are not isolated from vibration. The beam tube provides a 1.2-meter clear aperture to support multiple interferometer beams.

The beam tubes operate at  $10^{-9}$  Torr, principally limited by hydrogen outgassing from the steel, with much lower partial pressures of gases with higher polarizabilities. Because the hardware within the vacuum chambers is the major source of outgassing into the beam tubes, we concentrated pumping capacity near these chambers rather than distributing pumps along the beam tube. An extended bake-out of the completed vacuum tube was done and leaks in the 50 km of weld seams at each site were certified to be negligible. Each 2 km long tube segment was wrapped in a 15 cm thick layer of fiberglass insulation and baked at temperatures of 150–160 C for 3–4 weeks. Large magnet power supplies, on loan from Fermi National Accelerator Laboratory, fed approximately 1800 A of current through the length of the tubing to provide heat, while cryopumps were used temporarily along the length of the tubing to remove evolved gases. Post-bake accumulation measurements certified that  $H_2$  outgassing was below  $10^{-13}$  Torr  $l\text{ cm}^{-2}\text{ s}^{-1}$ , while water vapor and other species outgassed at rates between  $10^{-17}$  and  $10^{-20}$  Torr  $l\text{ cm}^{-2}\text{ s}^{-1}$ .

### 4. DESCRIPTION OF INITIAL INTERFEROMETERS

The initial interferometer [1] evolved from design principles successfully demonstrated with respect to minimizing displacement noise [2] and phase noise [3], and techniques for controlling laser frequency [4, 5], length [6, 7] and alignment [8, 9] in interferometer test beds. It uses a power-recycled, Fabry–Perot–Michelson configuration [6], shown schematically in figure 3. A laser system delivers light to the input optics, where further conditioning and stabilization of the light occurs. A beam splitter divides the light equally between the two arms. A 4 km (or 2-km) Fabry–Perot cavity is formed in each arm by a mirror in the corner station and a mirror in the end (or mid-) station. The cavities increase the phase shift per unit strain for the light reflected from the arms. The mirrors are suspended from a modular cage using a single loop of fine wire, allowing the mirrors to respond freely to gravitational waves. Magnets glued to the mirrors and voice coils attached to the cage are used for fine actuation of the mirrors. The suspension cages are attached to passive seismic isolation stacks [10] inside the vacuum chamber. Load forces are brought out of the vacuum chambers through support rods and bellows to an actuation system for coarse positioning and alignment. The interferometer is operated in a balanced state, with light resonating in the arms and then returning toward the laser source after recombining at the beam splitter, so the other port is in relative darkness. A photodetector in this 'dark port' detects any imbalance of the interferometer, but is insensitive to perturbations that affect both arms symmetrically. Feedback holds the interferometer in balance at all times and provides a measure of gravitational waves and any perturbations to the interferometer. The light returning toward the laser is recycled [11] by a power-recycling mirror to

increase light in the interferometer. A heterodyne detection scheme is used for sensing the cavity lengths and alignments throughout the interferometer. This involves impressing phase-modulation sidebands on the light at radio frequencies (RF), which are converted into amplitude modulations at various photodiodes by position and alignment errors between the light and the cavities. The interferometer sensitivity [12] will be limited by the seismic background below 35 Hz and by a thermal noise background [13, 14, 15] from 35 to 150 Hz. Above 150 Hz the strain noise is expected to increase linearly with frequency due to shot noise [16]. The noise-equivalent strain at 150 Hz is approximately  $3 \times 10^{-22}$ .

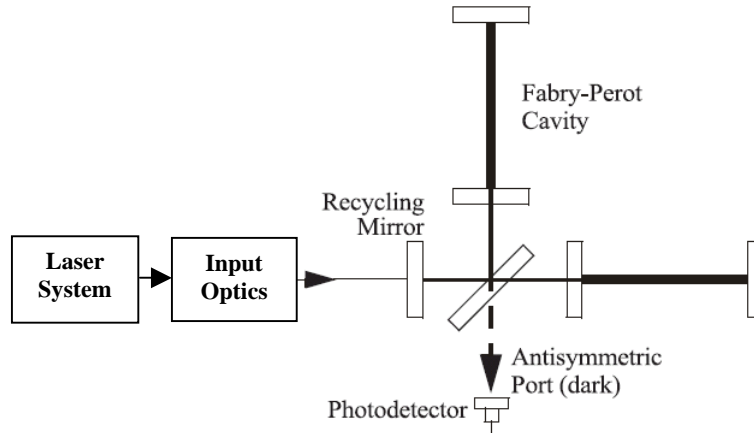


**Figure 3: Schematic of the initial interferometer, showing the long Fabry-Perot arms, beam splitter and recycling mirror of a main interferometer; a laser system supplies stabilized light that is further conditioned by the input optics system; the photodetector for the gravitational-wave output is shown.**

#### 4.1. Seismic isolation

A terrestrial interferometer requires vertical stiffness at low frequencies for support against Earth's gravity, but it should be free of Earth's motion in the gravitational-wave signal band. Seismic isolation provides freedom at signal frequencies, while a control system counteracts seismic activity at the lowest frequencies. The seismic isolation consists of "stacks" formed by several layers of massive leg elements separated by layers of coil springs with internal, constrained layers of damping material as shown in figure 4. Damping is required in the springs to limit motion on the stack resonances, which lie between 1.5 and 15 Hz. The damping material is sandwiched between aluminum slugs and the phosphor bronze walls, prior to coiling the springs. End caps are then e-beam welded onto the open ends of each coil to prevent contamination of the vacuum by the lossy damping material inside the spring. This results in a soft spring with mechanical  $Q \sim 30$ . The optical table supporting the suspension structures uses an internal space-frame structure to maintain high stiffness with low mass. We use a four-layer stack that supports an inverted optical table for the most demanding applications in the core optics of the interferometer. A three-layer stack supports the optical table used for the less demanding input optics. Transfer function measurements in air have verified good agreement with engineering models describing the stack resonances and in-vacuo measurements have verified isolation factors of more than  $10^6$  above 40 Hz for the four-layer stack that supports the most sensitive optics.

In addition, the systems at the ends of the arms are equipped with a fine actuator aligned with the arm that can translate the entire assembly (seismic isolation stack and optic suspension) along the optical axis by approximately  $\pm 90 \mu\text{m}$  over the frequency range from DC to  $\sim 10$  Hz. This system is used during the interferometer operation to compensate for earth tides, using a simple predictive model and a very slow feedback from the differential and common mode arm length controls. At LLO, an additional microseismic feed-forward system [17] was used to reduce the length fluctuations of the arms at the microseismic frequency (approximately 0.16 Hz). Also, the L1 detector's fine actuators were used together with seismometers in a beam-direction active seismic isolation system at each test mass chamber, which reduced seismic excitation of the most troublesome stack modes by a factor of  $\sim 5$ .



**Figure 4: Four-layer seismic stack (right), with inverted optical table resting upon top layer of springs; a pair of springs (upper left), ~7.5 cm high prior to compression; spring coil cross section (lower left) shows internal damping material constrained between internal slug and outer spring wall.**

#### 4.2. Mirror suspension

A gravitational wave produces displacements between inertial frames. Suspended mirrors serve as approximate markers for the inertial frames, whose positions can be read out by laser interferometry. If no forces were applied to the mirrors, they would remain fixed to inertial frames at all times, but this is not possible in earth-based detectors, because of earth's gravity. A mirror, suspended as a pendulum, is subject to a force from tension in the suspension fiber, but is asymptotically free to move in the directions transverse to the suspension fiber at frequencies above the natural frequency of the pendulum.

Ideally, no other forces would be applied to the mirrors at signal frequencies along the anticipated signal direction (i.e., path of light beam), because these applied forces can communicate noise into the mirror positions. However, the mirrors need to be held precisely in correct position and alignment over long time scales to allow a high-precision readout of mirror displacements by laser interferometry. Forces and torques on the mirrors will be needed both to bring the mirrors into initial position and alignment and to counteract background displacements of mirrors expected to come from residual seismic noise and thermal noise. Additional displacements may arise through these applied control forces and through "back action" from the light used to sense the mirror displacements.

In the LIGO detectors, mirrors are suspended in a modular cage with provisions for coarse sensing and control of the mirror position and alignment. The suspension cage attaches to either the top or bottom surface of a vibration-isolated optical table. Various features of a suspended mirror are shown in figure 5. A mirror is suspended by a single loop of steel music wire from a suspension block with grooved wire standoffs between the suspension wire and the mirror. The wire rests in the standoff grooves and the pitch angle of the mirror is adjusted coarsely to approximately  $10^{-4}$  radians of its specified angle by careful positioning of the wire standoffs, before they are glued onto the mirror. Care in making wire contacts to the mirror and clamps allows losses of  $< 10^{-5}$  in pendulum and violin modes of the suspended mirrors, consistent with thermal noise requirements. The mirror is damped and actuated by sensor/actuator heads, which are attached to the cage, and magnet/standoff assemblies, which are glued to the mirror. The mirror is protected during operation or held during transfer with safety stops attached to the cage.

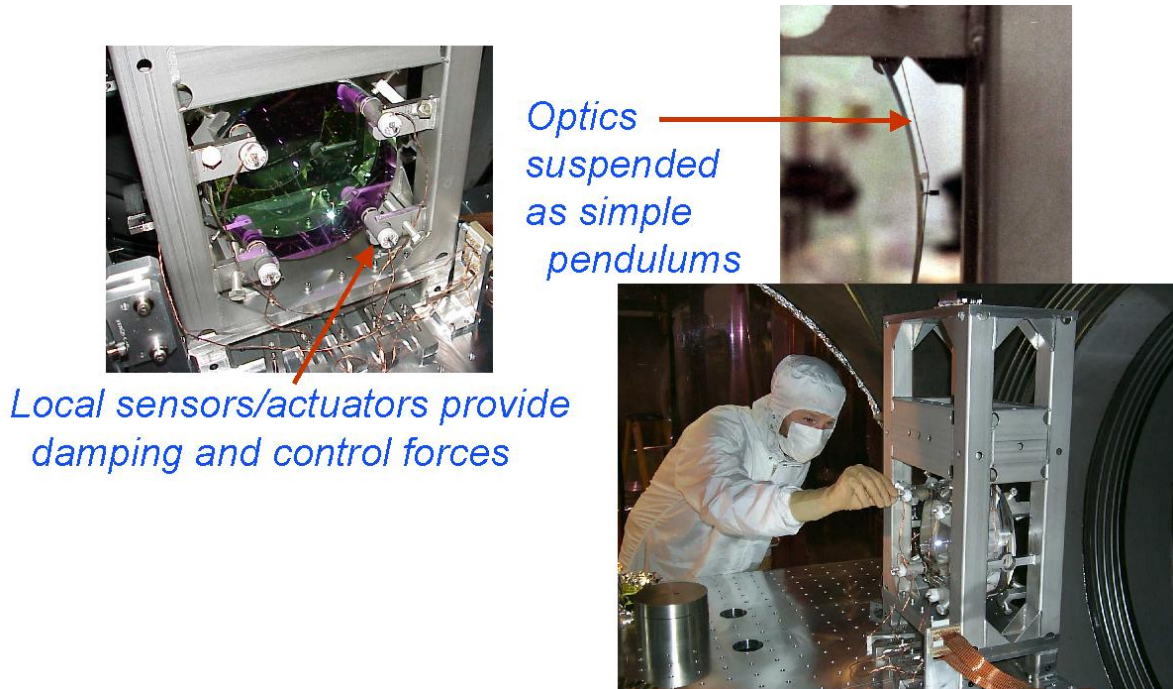


**Figure 5: A suspended mirror assembly (lower right) with suspension-wire detail and magnet assembly (upper right); shadow-sensor/voice-coil-actuator heads attach to the cage opposite the magnets (left) to provide for positioning, aligning and damping mirrors.**

### 4.3. Mirrors

The main interferometer mirrors[18,19] are fabricated from high-purity fused silica, 25 cm in diameter and 10 cm thick (except the beam splitter which is 4 cm thick). Radii of curvature of the cavity optics are chosen so that the arm cavities have a stability  $g = (1 - L/R_1)(1 - L/R_2)$  ( $L$  is the cavity length and  $R_n$  are the radii of curvature of the two cavity mirrors) of 0.33 (H1 and L1) or 0.67 (H2), to minimize the excitation of higher order transverse modes by separating them in frequency from the laser frequency and its RF modulation sidebands. The surface figure accuracy of the polished optic is better than 1 nm; the coatings have a thickness uniformity that holds their contribution to the apparent surface flatness negligible. The coatings have a power absorption less than 1 ppm and scatter less than 70 ppm. All optics are wedged (typically about 2 degrees) to reduce the possibility of stray reflections interfering with the main beam and to give access to samples of the light inside the interferometer. Transmission of the input mirrors to the arm cavities is 2.7% and the end mirrors have a transmission of approximately 12 ppm, to give an arm cavity pole frequency of 85 Hz (170 Hz for H2). The beam-splitter reflectivity was specified as  $50 \pm 0.5\%$ . The recycling mirror transmission is also 2.7%, to give a design recycling factor (or increase in the circulating power) of  $\sim 50$  for the optics as designed and at full power.

The mirrors must also have low mechanical losses to prevent energy from internal mechanical resonances in equilibrium at room temperature from leaking into the signal band. Mirror thickness was chosen so that potentially troublesome modes are above the signal band. Mechanical losses of the fused silica substrate are of order  $10^{-6} - 10^{-7}$ , consistent with design expectations. We expect that the main contribution to the thermal noise will arise from the dielectric mirror coatings[15], but measurements and analysis indicate that these losses are low enough to reach the initial detector sensitivity goal.

#### 4.4. Laser system and input optics

A pre-stabilized laser system (PSL) and the input optics (IOO) supply conditioned laser light to the interferometer. The PSL (figure 6) incorporates a 10 W, diode-pumped, Nd:YAG laser [20], developed for LIGO by Lightwave Electronics. A sample of light from this laser is frequency shifted and locked to a reference cavity using the standard RF reflection locking technique [4]. The main light beam is passed through a small mode-cleaning cavity (pre-mode cleaner or PMC) to improve its power stability and beam shape and then enters the input optics for further filtering and beam conditioning. The laser system has inputs for active power stabilization and frequency correction. At very low frequencies, the temperature of the reference cavity may be adjusted for common-mode compensation of the Earth's tide. PSL is phase modulated for locking to subsequent cavities and then injected into the main vacuum system.

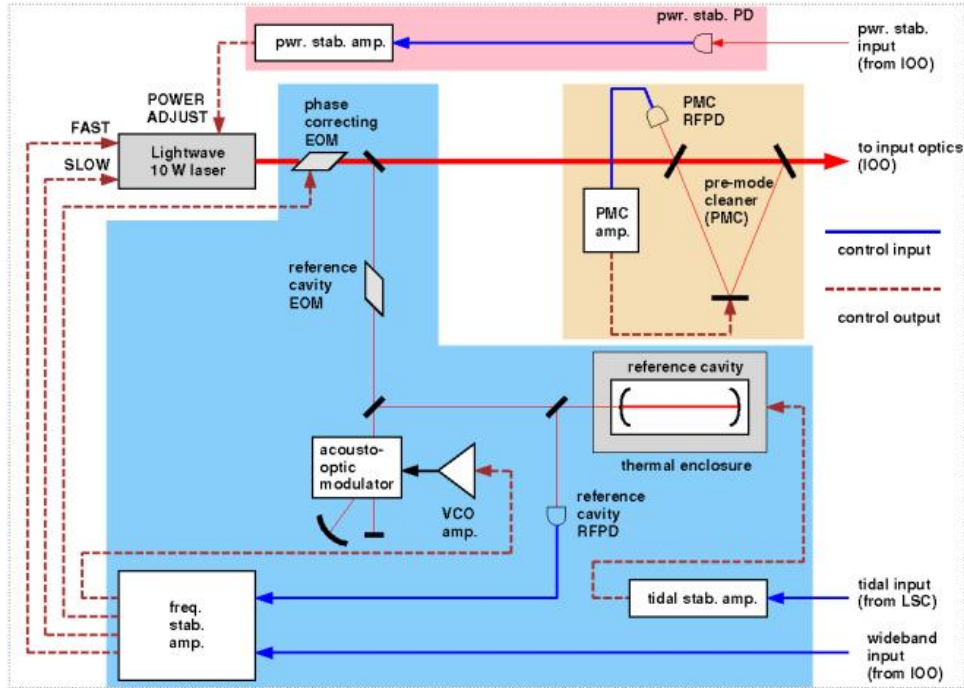


**Figure 6: Schematic of the pre-stabilized laser system, showing the reference cavity leg for stabilizing frequency and the pre-mode cleaner to filter the main light output for improved mode quality.**

The input optics system provides conditioning of the light and injects the light into the main interferometer. Output from the pre-mode cleaner is passed through a bank of pockels cell to apply phase-modulation sidebands at RF frequencies (typically tens of Megahertz). A triangular mode-cleaning cavity [21], formed by separately suspended mirrors on vibration-isolated tables, is used in transmission to further stabilize the frequency, amplitude and mode quality of the light. This mode cleaner has a length of 12–15 m, tuned to the RF modulation sidebands that are transmitted with the carrier light for detection of cavity lengths and wavefront errors in the main interferometer. A three-element, suspended-mirror reflection telescope is used to mode match and align the light to the long Fabry-Perot cavities in the interferometer arms.

Laser power stabilization signals can be returned to the laser from before or after the mode cleaner as necessary. In addition, once the main interferometer is locked, frequency stabilization corrections to the laser are derived from the average length of the two Fabry-Perot cavities in the arms.

#### 4.5. Control system

The interferometer control system needs to bring the critical optical surfaces into proper alignment and position and then maintain these parameters against disturbances from the physical environment. The pre-stabilized laser system provides some stabilization of frequency and intensity, but these must be further tuned and matched to the main interferometer. Approximately 100 control systems bring the interferometer from an uncontrolled state to its running state. These are listed in Table 1. The stringent requirements of this final state include controlling arm lengths to  $10^{-13}$  meters RMS and alignment angles to  $10^{-8}$  radians.

**Table 1: Listing of control systems for a single interferometer**

Function	Degrees of freedom	Implementations	Number/Function
Shadow sensor damping	4	14	56
Optical lever damping	2	7	14
Laser pre-stabilization	3	1	3
Cavity length control	6	1	6
Wave-front control	2	7	14
Beam-centering control	2	3	6
<b>Total Number</b>			<b>99</b>

Integrated shadow sensors and voice coils are used to damp suspended-mirror motion to the frame of the suspension cage. This allows damping of mirror pitch and yaw and position along the optic axis and horizontally transverse to the axis. Shadow sensor damping provides sufficient angular stability to allow optical lever damping to operate. Optical-lever lasers illuminate a subset of mirrors and their reflections are captured on quadrant photodiodes, whose position are fixed to the facility floor several meters away. The optical lever signals in pitch and yaw are fed back to the voice coils to damp these angular degrees of freedom to the floor of the local building, removing angular fluctuations due to low-frequency resonances in the seismic isolation stacks. Optical lever damping provides sufficient angular stability to allow light to reflect multiple times between mirrors at opposite ends of the long arms, to produce overlapping beam spots and intermittent interference fringes. The pre-stabilization system for the laser provides stabilization of the laser frequency to an isolated reference cavity, transmission of the light through a filter cavity (pre-mode cleaner) to clean up the modal content of the light and intensity stabilization of the laser light. Length control includes resonating the light in the mode-cleaner cavity, controlling the two arm lengths, positioning the beam splitter and the recycling mirror. Additionally, the laser frequency is corrected to match the average length of the two long arms. These functions require sequential lock acquisition (or “locking”) of the loops controlling various degrees of freedom of the length control system. This is accomplished by detecting transient passages through resonances and actuating on the mirrors and laser to stretch the duration of these transients until stable operation can be obtained. A lock acquisition code[22] has been developed by simulation and measurement that automatically senses the state of resonances in various arms and configures the length controls appropriately to acquire lock. Once the interferometer cavity lengths are stably controlled and matched to the laser frequency, the gradients of optical phase on the light at various points can be measured. This information is used by the wave-front control system to trim the alignment of the mirrors to the incident laser light. A combination of quadrant diodes and cameras monitors the position of the beam spots on the mirrors. This information is used by the beam-centering control system to center the beams on the beam splitter and the two end mirrors.

The control systems use analog sensors, whose signals are whitened and digitized. Control loop configuration and gain shaping are done digitally and applied to a digital-to-analog converter. This output is filtered to remove digital artifacts and applied to the appropriate actuator. This architecture allows stable maintenance of a large range of filter variables, implementation of stepped operations and non-linear functions and simple reconfiguration of the controls. A graduate student can download control system parameters into a simulation program on a laptop, simulate performance and test a reconfigured control loop and upload the new system in several hours. This agility is extremely important on such a complex control system and has allowed rapid progress in improving sensitivity.

#### 4.6. Data acquisition, archiving and diagnostics

The LIGO data stream includes not only the gravitational wave channel and the control system channels from each interferometer but also data from an extensive array of sensors that characterize the physical environment in which the interferometers operate. Computers distributed throughout the site acquire the data using 16-bit ADCs, with time stamps provided by GPS receivers in each building. A separate atomic clock at each observatory allows for independent comparisons with the GPS system and timing diagnostics. The overall data rates are  $\sim 3$  MB/s for Livingston and  $\sim 5$  MB/s for Hanford. A central computer collects this data into data structures, called frames, that employ a common format used by the various international detector groups. The frames are available on disk for analysis or diagnostics and are archived for later distribution throughout the collaboration. Each observatory also has an online data analysis capability, using a BEOWULF parallel computing architecture, with up to 280 processors.

Extensive diagnostic software is available to operate on the data. A global diagnostic system includes software tools for time-domain and frequency-domain analysis of any set of data channels. Additionally, it provides an arbitrary waveform generator that can apply test signals and measure response functions. The global diagnostic system is used for detailed studies. A data monitoring tool system is also available for “on-the-fly” characterization and trending of system performance. This system includes high-bandwidth, low-latency access to the data and independent processors on a fast network, with specialized software to provide up-to-date displays of machine performance in the control room.

### 5. OPERATIONS

Observatory construction began with rough grading of the observatory sites in 1994 and 1995, followed by detail design of the facilities. Major facility construction began in 1996 and laboratory spaces became available for equipment in 1997 and 1998. Figure 7 provides a timeline of detector commissioning following the inauguration of completed facilities in autumn, 1999.

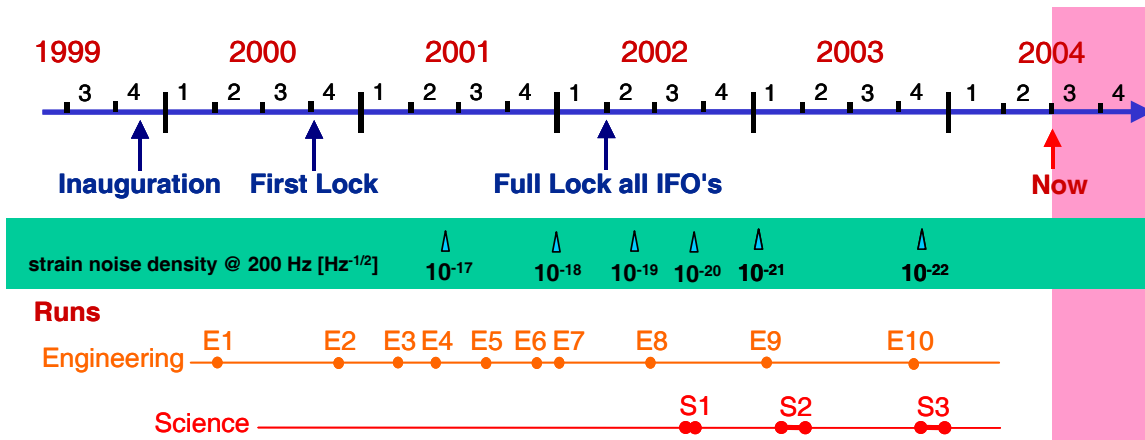


**Figure 7: Timeline of LIGO commissioning and science runs.**

The first laser light transited one of the evacuated arms for the Hanford 2 km interferometer in late November 1999. The initial shots down each arm landed within 25 cm of the mirror center, verifying the accuracy of the alignment procedures, from an initial site survey through final optical alignment. Residual voice coil actuation of the mirrors was sufficient to bring the arms into full alignment. Each of the 2 km Fabry–Perot arms at Hanford were separately locked into optical resonance using a single, temporary, analog control system and measurements were made to characterize environmental influences and to verify the optical performance predicted from laboratory measurements. The first engineering run (E1), a 20 h data run utilizing a single locked arm, was taken during the first week of April 2000. This inaugurated a series of engineering runs used to test the interferometer under extended running conditions as the

hardware and control systems were brought on line. The Hanford 2 km, power-recycled, Fabry–Perot Michelson interferometer was locked for the first time by October 2000 and characterization of lock acquisition and robustness were begun. Five days of data were taken in a recombined mode, with no power recycling, during a one-week engineering run (E2) in November. The duty cycle for data obtained in this configuration was approximately 95%, and 2 terabytes of interferometer, system and environmental data were recorded. Loss of lock was principally due to the Earth’s tide, in good agreement with a predictive tidal model. Engineering runs E2 through E7 tested various configurations of the three LIGO interferometers, data acquisition and archiving systems in coincidence operation. By early 2002, all interferometers had been operated in a power-recycled, Fabry–Perot Michelson configuration.

By the middle of 2002, interferometer sensitivity had been improved by three orders of magnitude above initial results as subsystem troubleshooting improved and the control system was implemented and tuned. At this point, a scientific

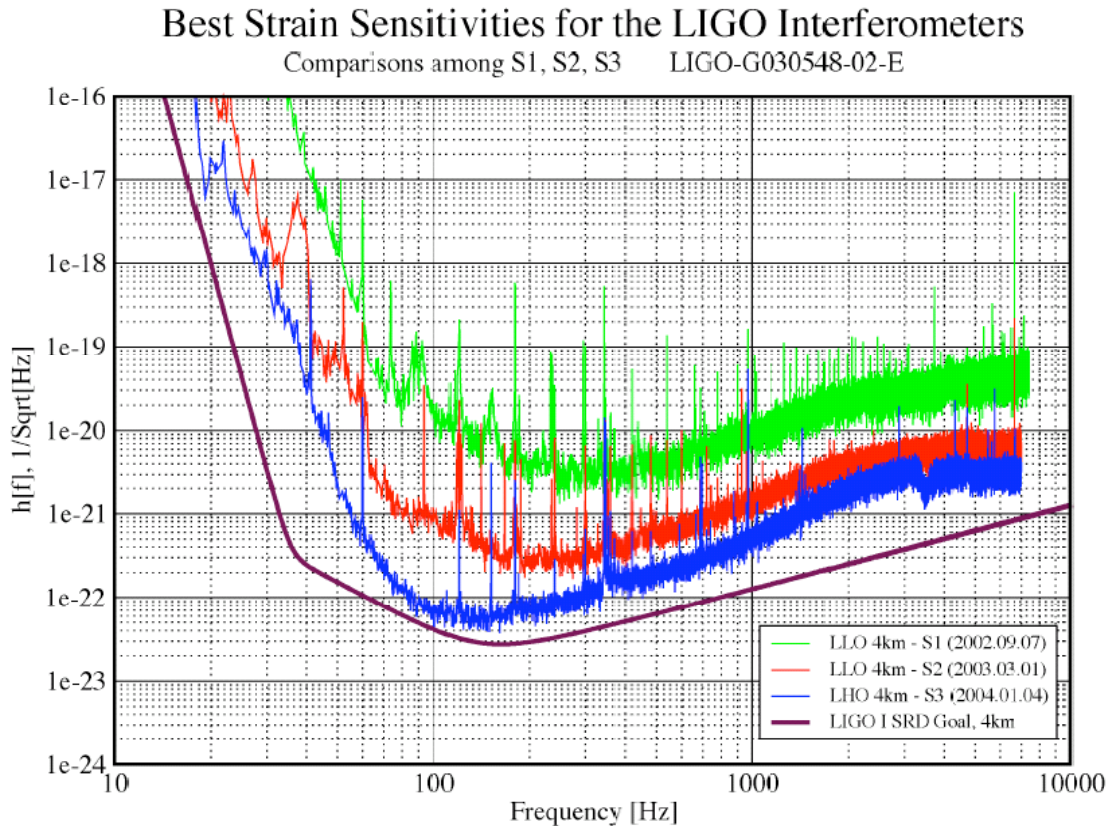


**Figure 8: Strain sensitivity for various runs.**

observing run (S1) was scheduled for 17 days in August and September of 2002, with three LIGO interferometers and GEO600 in coincident operation[23]. This was followed by two subsequent science runs: S2 from February 14 to April 14, 2003 and S3, from October 31, 2003 to January 9, 2004. Figure 8 shows the spectra for the most sensitive interferometer in each of these runs, compared to the sensitivity goal for the initial interferometers.

We use the waveform for two inspiralling neutron stars, of 1.4 solar masses each, as a benchmark waveform to derive a figure of merit for these broad band detectors: the range to which we can typically make a high-confidence detection of such an event. (Neutron star inspirals were chosen because the waveform is well known and it extends across the broad band of detector response.) This inspiral range metric has improved steadily as the interferometer strain sensitivity has been increased and extended to lower frequencies. The best interferometer in S1 had a range covering the Milky-Way Galaxy and the Magellanic Clouds. By S2, the range included the Andromeda Galaxy (M31) at  $\sim 1$  Mpc and by S3, the range covered a significant fraction of the distance to the Virgo supercluster.

The reliability of the interferometers during the S3 science run can be seen in figure 9, which shows how the inspiral range varied for each interferometer, as well as the overall duty cycles for the run. Duty cycles for the interferometers at

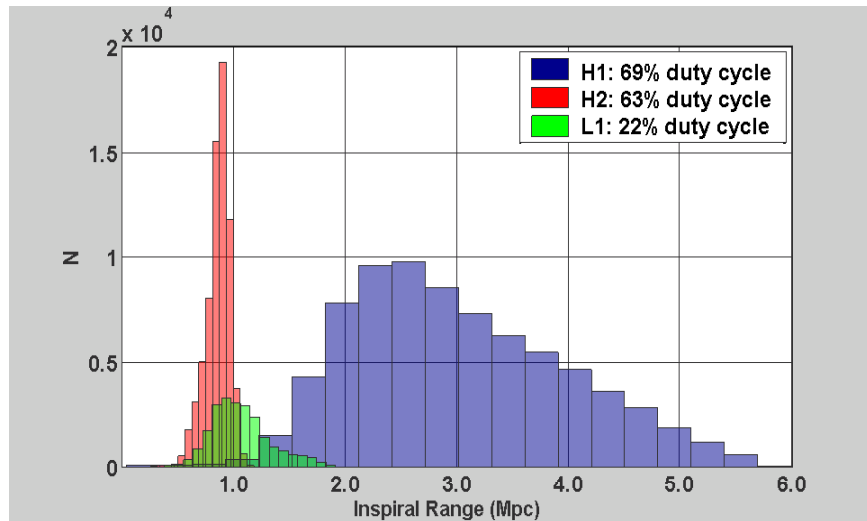


**Figure 9: Binary neutron star range and duty cycle for S3 run.**

Hanford typically ran 60-70%, compared to our goal of 90%. Livingston duty cycle was much lower, principally due to larger ground noise most days caused by logging of the surrounding forest. A major upgrade to the Livingston interferometer's seismic isolation is currently underway to extend the duty cycle in the presence of these higher vibration levels. Implementation of a system to reduce the influence of the microseism at Hanford should improve duty cycles there for future runs.

A model for the limiting noise affecting the sensitivity of the H1 interferometer is shown in figure 10, evaluated for November 24, 2003, during science run S3. The plot shows the displacement noise in meters divided by the square root of the channel bandwidth as a solid black line. The initial detector sensitivity goal is also shown for comparison. The goal curve is limited by seismic background noise at frequencies below 40 Hz, by shot noise at high frequencies and by thermal noise in the intermediate frequency region. An experimental estimate of seismic noise using measurements of ground noise and measured properties of the seismic isolation system is close the goal level. A phenomenological estimate of the shot noise level during S3 agrees with the observed noise between 200 Hz and 1 kHz. Above 1 kHz, the interferometer noise agrees well with an estimate of the effect of phase noise from the oscillator used to apply the RF sidebands to the light used for the length control system. At low frequencies, an estimate of the effect of noise in the auxiliary control loops that determine the position of the beam splitter and the power-recycling mirror agrees well with the observed noise. These noise estimates explain the observed sensitivity, except in the frequency regime between 70 Hz and 150 Hz. The noise in this region was observed to vary during the run, causing the large variations in estimated neutron star inspiral range shown in figure 9. The nature of this noise will be investigated further. Once the dominant noise sources in the control system are diagnosed and reduced we expect other noise sources to become observable. Some of these have been estimated but are not shown in figure 10 for clarity. Using a lower noise oscillator will reduce the noise above 1 kHz, but we expect then to encounter noise due to residual laser frequency fluctuations near 6 kHz. Changes to the frequency stabilization control loops should reduce this noise. To reduce shot noise, we are testing an output mode cleaner that should prevent higher-order spatial modes of the light at the gravitational wave output port from reaching the photodiode. There is significant power in these higher-order modes that does not contribute to the optical gain of the differential control loops, but which does produce shot noise and can also introduce offsets into the control loop. Similarly, we know that there is noise coming from the wavefront control system that lies below the current noise from the auxiliary length control loops at low frequencies. This noise source is expected to become important once the noise from the auxiliary loops is reduced.

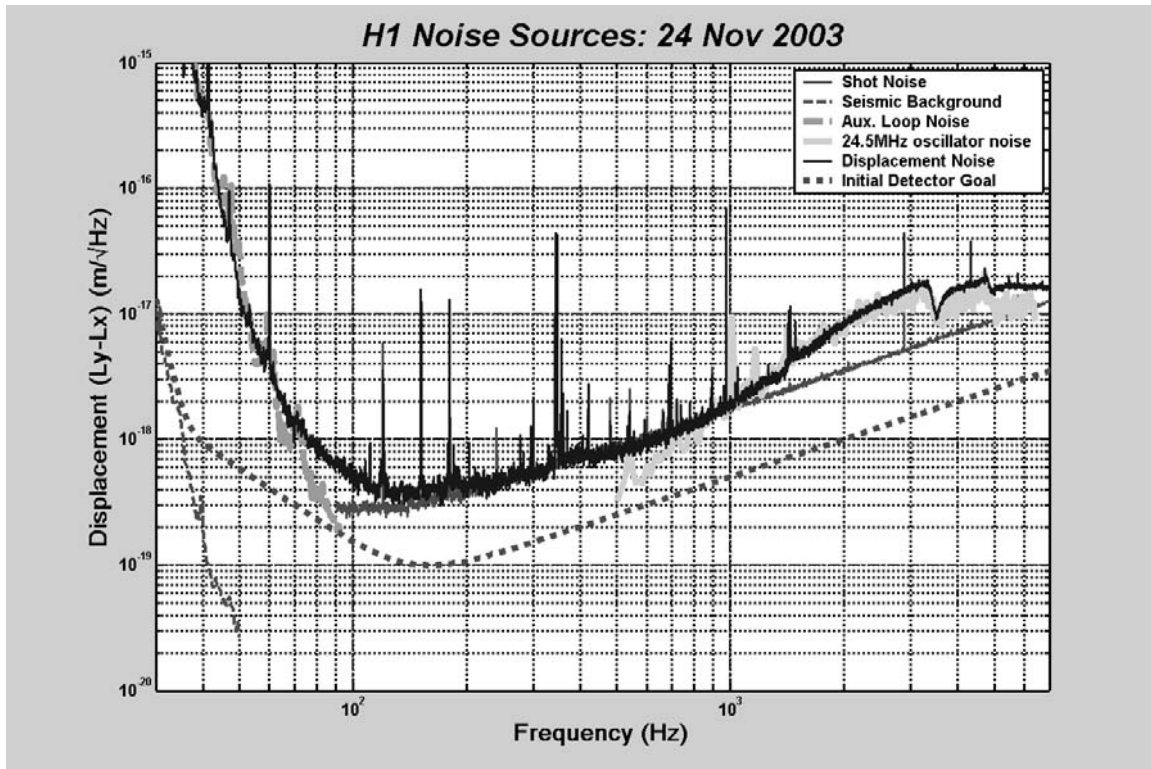


Figure 10: Limitations to H1 noise during S3 run.

## 6. ASTROPHYSICAL RESULTS

Astrophysical analysis of LIGO data is divided into four broad classes:

- Searches for periodic sources, such as gravitational radiation from pulsars.
- Searches for compact binary inspiral waveforms, such as the radiation from pairs consisting of neutron stars, black holes and machos.
- Searches for burst sources, whose waveforms may be unknown or poorly known. These searches may include triggers from other astronomical detectors, such as supernova or gamma-ray burst observations.
- Searches for stochastic gravitational waves of cosmological or astrophysical origin.

Analysis results from the S1 science run are now appearing in the literature. As evident from figure 8, the sensitivity of the interferometers for S1 was far from design sensitivity and it is not surprising that this analysis only provided upper limits on the strengths of gravitational waves from these sources. Nonetheless, the S1 data have allowed us to hone our analysis techniques on real data and have produced the most stringent limits to date on many classes of sources.

The search for periodic gravitational waves from known radio pulsars is typically done by using a time domain method, whereas searches for new pulsars – whose frequencies and sky coordinates are unknown – will rely on hierarchical search techniques in the frequency domain. Data from the three LIGO interferometers and from GEO600 were combined to search for gravitational wave emission from J1939+2134, using both time and frequency methods[24]. Data from S2 and S3 are now being analyzed to search for waves from all known radio pulsars, from SCO-X1, and a search for new pulsars near the center of our galaxy.

A search through the S1 data has been conducted for the inspiral waveforms from two neutron stars [25], by correlation of the data against search template waveforms. Searches through S2 and S3 data are ongoing and more computationally demanding searches, covering black holes and machos are under way.

A search for generalized bursts of gravitational waves, using time-domain and time-frequency methods to search for anomalies that are correlated in the three LIGO interferometers, was done using the S1 data [26]. Data from S2 and S3 are being analyzed for generalized bursts and for black-hole ringdown waveforms. A triggered search for gravitational wave emission from GRB030329 – a strong gamma-ray burst detected during the S2 science run – is also underway.

A search for stochastic gravitational waves using the S1 data has been completed [27], by correlating the output of the Hanford and Livingston interferometers. The sensitivity of a two-site correlation depends heavily on the low-frequency sensitivity of the interferometers, because the phases of higher-frequency correlations from different parts of the sky cancel. Better low-frequency performance of the detectors in S2 and S3 will greatly increase the sensitivity of this all-sky stochastic search. Additionally, measures taken prior to S3 to reduce acoustic cross-coupling of the two co-located interferometers, H1 and H2, should allow good limits to be obtained over a broader range of frequencies.

## 7. ACKNOWLEDGEMENT

Our collaboration gratefully acknowledges the support of the United States National Science Foundation for the construction and operation of the LIGO Laboratory and the Particle Physics and Astronomy Research Council of the United Kingdom, the Max-Planck-Society and the State of Niedersachsen/Germany for support of the construction and operation of the GEO600 detector. We also gratefully acknowledge the support of their research by these agencies and by the Australian Research Council, the Natural Sciences and Engineering Research Council of Canada, the Council of Scientific and Industrial Research of India, the Department of Science and Technology of India, the Spanish Ministerio de Ciencia y Tecnologia, the John Simon Guggenheim Foundation, the David and Lucile Packard Foundation, the Research Corporation, and the Alfred P. Sloan Foundation. This paper has been issued LIGO document number P040019-00-R.

## REFERENCES

1. A. Abramovici, et al, “The laser interferometer gravitational-wave observatory”, *Science*, **256**, 325–33, (1992).
2. A. Abramovici, et al, “Improved sensitivity in a gravitational wave interferometer and implications for LIGO”, *Phys. Lett. A*, **218**, 157–63, (1996).
3. P. Fritschel, G. Gonzalez, B. Lantz, P. Saha and M. Zucker, “High power interferometric measurement limited by quantum noise and application to detection of gravitational waves”, *Phys. Rev. Lett.*, **80**, 3181–4, (1998).
4. R.W.P. Drever, J.L. Hall, F.W. Kowalski, J. Hough, G.M. Ford, A.J. Munley and H. Ward, *Appl. Phys. B*, **31**, 97, (1983).
5. G.A. Kerr, N.A. Robertson, J. Hough and C.N. Man, *Appl. Phys. B* **37**, 11, (1985); S. Kawamura, A. Abramovici and M.E. Zucker, “Improved multistage wide band frequency stabilization”, *Rev. Sci. Instrum.*, **68**, 223–9, (1997).
6. D. Shoemaker, P. Fritschel, J. Giaime, N. Christensen and R. Weiss, “Prototype Michelson interferometer with Fabry–Perot cavities”, *Appl. Opt.*, **30**, 3133–8, (1991); M.W. Regehr, F.J. Raab and S.E. Whitcomb, “Demonstration of a power-recycled Michelson interferometer with Fabry–Perot arms by frontal modulation”, *Opt. Lett.*, **20**, 1507–9, (1995); R. Flaminio and H. Heitman, “Longitudinal control of an interferometer for the detection of gravitational waves”, *Phys. Lett. A*, **214**, 112–22, (1996); D. Sigg, N. Mavalvala, J. Giaime, P. Fritschel and D. Shoemaker, “Signal extraction in a power recycled Michelson interferometer with Fabry–Perot arm cavities by use of a multiple-carrier frontal modulation scheme”, *Appl. Opt.*, **37**, 5687–93, (1998).
7. J. Camp, L. Sievers, R. Bork and J. Heefner, “Guided lock acquisition in a suspended Fabry–Perot cavity”, *Opt. Lett.*, **20**, 2463–5, (1995).
8. S. Kawamura and M.E. Zucker, “Orientation noise in a Fabry–Perot interferometer gravitational wave detector”, *Appl. Opt.*, **33**, 3912–8, (1994); N. Mavalvala, D. Sigg and D. Shoemaker, “Experimental test of an alignment sensing scheme for a gravitational wave interferometer”, *Appl. Opt.*, **37**, 7743–6, (1998); D. Sigg and N. Mavalvala, “Principles of calculating the dynamical response of misaligned complex optical interferometers”, *J. Opt. Soc. Am. A*, **17**, 1642–9, (2000).

9. D. Sigg and R.G. Beausoleil, "Spatiotemporal model of a LIGO interferometer", *J. Opt. Soc. Am. A*, **16**, 1642–9, (1999).
10. J. Giaime, P. Saha, D. Shoemaker and L. Sievers, "A passive vibration isolation stack for LIGO: design, modeling and testing", *Rev. Sci. Instrum.*, **67**, 208–14, (1996).
11. R.W.P. Drever, "Interferometric detectors for gravitational radiation", *Gravitational Radiation*, N. Deruelle and T. Piran, pp 321–8, North-Holland, Amsterdam, (1983); B.J. Meers, "Recycling in laser-interferometric gravitational-wave detectors", *Phys. Rev. D*, **38**, 2317–26, (1988).
12. R. Weiss, "Electromagnetically coupled broadband gravitational antenna", *Q. Prog. Rep. Res. Lab. Electr.MIT*, **105**, 54, (1972); K.S. Thorne, "Gravitational radiation", *300 Years of Gravitation*, S W Hawking and W Israel, pp 330–458, Cambridge University Press, Cambridge, (1987).
13. P.R. Saulson, "Thermal noise in mechanical experiments", *Phys. Rev. D*, **42**, 2437–45, (1990).
14. A. Gillespie and F. Raab, "Thermally excited vibrations of the mirrors of laser interferometric gravitational wave detectors", *Phys. Rev. D* **52** 577–85, (1995); A. Gillespie, "Thermal noise in the initial LIGO interferometers", *PhD Thesis*, California Institute of Technology, Pasadena, (1995).
15. Y. Levin, "Internal thermal noise in LIGO test masses: A direct approach", *Phys. Rev. D*, **57**, 659-663, (1998); G.H. Harry, A.M. Gretarsson, P.R. Saulson, S.E. Kittelberger, S.D. Penn, W.J. Startin, S. Rowan, M. Fejer, D.R.M. Crooks, G. Cagnoli, J. Hough and N. Nakagawa, "Thermal noise in interferometric gravitational wave detectors due to dielectric optical coatings", *Class. Quant. Grav.*, **19**, 897-917, (2002).
16. J. Vinet, B. Meers, C.N. Man and A. Brillet, "Optimization of long-baseline interferometers for gravitational wave detection", *Phys. Rev. D*, **38**, 433–47, (1988); T.M. Niebauer, R. Schilling, K. Danzmann, A. Rudiger and W. Winkler, "Nonstationary shot noise and its effect on the sensitivity of interferometers", *Phys. Rev. A*, **43**, 5022–9, (1991); T.T. Lyons, M.R. Regehr and F.J. Raab, "Shot noise in gravitational wave detectors with Fabry–Perot arms", *Appl. Opt.*, **39**, 6761–70, (2000).
17. J.A. Giaime, E.J. Daw, M. Weitz, R. Adhikari, P. Fritschel, R. Abbott, R. Bork, and J. Heefner, "Feedforward reduction of the microseism disturbance in a long-baseline interferometric gravitational-wave detector," *Rev. Sci. Instrum.*, **74**, 218-224, (2003).
18. S. Whitcomb, G. Billingsley, J. Carri, A. Golovitsner, D. Jungwirth, W. Kells, H. Yamamoto, B. Bochner, Y. Hefetz, P. Saha, and R. Weiss, "Optics development for LIGO," *Proceedings of the TAMA International Workshop on Gravitational Wave Detection*, K. Tsubono, M.-K. Fujimoto, and K. Kuroda, 229- 239, Universal Academy Press, Tokyo, (1997).
19. C.J. Walsh, A.J. Leistner, J. Seckold, B.F. Oreb, and D.I. Farrant, "Fabrication and measurement of optics for the laser interferometer gravitational wave observatory," *Appl. Optics*, **38**, 2870-2879, (1999).
20. R.L. Savage Jr, P.J. King and S.U. Seel, "A highly-stabilized 10W Nd:YAG laser for the laser interferometer gravitational-wave observatory (LIGO)", *Laser Phys.* **8**, 679–85, (1998).
21. A. Rudiger, R. Schilling, L. Schnupp, W. Winkler, H. Billing and K. Maischberger, *Opt. Act.* **28** 641, (1981).
22. M. Evans, N. Mavalvala, P. Fritschel, R. Bork, B. Bhawal, R. Gustafson, W. Kells, M. Landry, D. Sigg, R. Weiss, S. Whitcomb and H. Yamamoto, "Lock acquisition of a gravitational-wave interferometer", *Optics Lett.*, **27**, 598-600, (2002).
23. The [LIGO Scientific Collaboration: B. Abbott](#), et al, "Detector description and performance for the first coincidence observations between LIGO and GEO", *Nucl.Instrum.Meth.*, **A517**, 154-179, (2004).
24. The [LIGO Scientific Collaboration: B. Abbott](#), et al, "Setting upper limits on the strength of periodic gravitational waves using the first science data from the GEO600 and LIGO detectors", *Phys.Rev.*, **D69**, 082004, (2004).
25. The [LIGO Scientific Collaboration: B. Abbott](#), et al, "Analysis of LIGO data for gravitational waves from binary neutron stars", gr-qc/0308069.
26. The [LIGO Scientific Collaboration: B. Abbott](#), et al, "First upper limits from LIGO on gravitational wave bursts", gr-qc/0312056, accepted by **Phys.Rev.D**, (2004).
27. The [LIGO Scientific Collaboration: B. Abbott](#), et al, "Analysis of First LIGO Science Data for Stochastic Gravitational Waves", gr-qc/0312088.